EPJ manuscript No.
(will be inserted by the editor)

On the ΣN cusp in the $pp \to pK^+\Lambda$ reaction

S. Abd El-Samad[1], E. Borodina[2,3], K.-Th. Brinkmann[4], H. Clement[5,6], E. Doroshkevich[5,6], R. Dzhygadlo[2,3], K. Ehrhardt[5,6], A. Erhardt[5,6], W. Eyrich[7], H. Freiesleben[8], W. Gast[2,3], A. Gillitzer[2,3], D. Grzonka[2,3], C. Hanhart[2,3,9], F. Hauenstein[2,3,7], P. Klaja[2,3,7], K. Kilian[2,3], M. Krapp[7], J. Ritman[2,3], E. Roderburg[2,3], M. Röder[2,3], M. Schulte-Wissermann[7], W. Schroeder[2,3,7a], T. Sefzick[2,3], G.J. Wagner[5,6], P. Wintz[2,3], and P. Wüstner[2,3,10]

[1] Atomic Energy Authority NRC Cairo, Egypt
[2] Institut für Kernphysik, Forschungszentrum Jülich, D-52428 Jülich, Germany
[3] Jülich Center for Hadron Physics, Forschungszentrum Jülich, D-52428 Jülich, Germany
[4] Physikalisches Institut Justus-Liebig-Universität, D-35392 Gieβen,Germany
[5] Physikalisches Institut der Universität Tübingen, Germany
[6] Kepler Center for Astro and Particle Physics, University of Tübingen, Auf der Morgenstelle 14, D-72076 Tübingen, Germany
[7] Friedrich-Alexander-Universität Erlangen-Nürnberg, D-91058 Erlangen, Germany
[8] Institut für Kern- und Teilchenphysik, Technische Universität Dresden, D-01062 Dresden, Germany
[9] Institute for Advanced Simulation, Forschungszentrum Jülich, D-52428 Jülich, Germany
[10] Zentralinstitut für Elektronik, Forschungszentrum Jülich, D-52428 Jülich, Germany
(COSY-TOF Collaboration)

April 24, 2018

Abstract. Measurements of the $pp \to pK^+\Lambda$ reaction at $T_p = 2.28$ GeV have been carried out at COSY-TOF. In addition to the Λp FSI and N^* resonance excitation effects a pronounced narrow structure is observed in the Dalitz plot and in its projection on the $p\Lambda$-invariant mass. The strongly asymmetric structure appears at the $pp \to NK^+\Sigma$ threshold and is interpreted as ΣN cusp effect. The observed width of about 20 MeV/c^2 is substantially broader than anticipated from previous measurements as well as theoretical predictions. Angular distributions of this cusp structure are shown to be dissimilar to those in the residual $pK^+\Lambda$ channel, but similar to those observed in the $pK^+\Sigma^0$ channel.

PACS. 13.75.Cs – 13.75.Ev – 14.20.Jn – 14.20.Pt – 25.10.+s – 25.40.Ep

1 Introduction

The hyperon production in nucleon-nucleon collisions has attracted interest in recent years for a number of reasons. First, it offers a valuable tool for the determination of the hyperon-nucleon final state interaction (FSI). Most directly this effect is seen in the hyperon-nucleon invariant mass spectrum. For a recent determination of the Λp-FSI by the COSY-HIRES collaboration using a high-resolution magnetic spectrometer see Ref. [1]. Second, it gives access to the rare decay branches of N^* resonances produced in the NN collisions. For recent work on that see Refs. [2, 3, 4, 5, 6]. Third, it offers the chance to search for more exotic objects like pentaquarks [7, 8, 9] or dibaryons [10, 11]. Among the latter an inevitable, though not very exotic candidate would be the ΣN system produced near threshold followed by a $\Sigma N \to \Lambda N$ transition. Whenever an inelastic channel opens in a production reaction, it produces a non–analyticity in the spectra, a so-called cusp, the strength of which is a measure of the corresponding transition matrix element (here $\Sigma N \to \Lambda N$) - *e.g.* see Ref. [13] for the method to extract the s-wave $\pi\pi$ scattering lengths from $K \to 3\pi$. Signs of such a cusp in the $pp \to pK^+\Lambda$ reaction have been first observed in inclusive measurements with single-arm magnetic spectrometers at Saclay [12] and COSY-HIRES [14]. A theoretical calculation of this cusp effect in proton-proton collisions has been presented by Laget [15].

Originally a peak structure at the position of the ΣN threshold has been discovered in K^- absorption in deuterium [16]. Subsequent bubble-chamber measurements [17, 18] observed a pronounced peak at the Σ threshold with a width of about 10 MeV/c^2 and below. For a review and a discussion of possible dibaryon aspects see, *e.g.* Refs. [19, 20, 21, 22].

In exclusive and kinematically complete COSY-TOF measurements indications of this cusp have been observed at several energies [4, 5, 6]. Since these measurements lack the necessary statistics for a reliable investigation of the cusp effect, we use here the measurements at $T_p = 2.28$ GeV

[a] present address: Forschungszentrum Jülich, D-52428 Jülich, Germany
Correspondence to: H. Clement
email: clement@pit.physik.uni-tuebingen.de

(p = 3.081 GeV/c) for a detailed investigation of this matter. The primary purpose of this run, which comprises an order of magnitude higher statistics than the previous TOF-measurements, was originally the pentaquark search [7]. Angular distributions obtained from this run have been published already for both $pK^+\Lambda$ and $pK^+\Sigma^0$ channels [2]. The results presented in this paper are based on the thesis work of Refs. [23,24], where also details of experiment and analysis are found.

2 Experiment

2.1 Detector setup

Since the experimental setup was discussed in detail already in Refs. [2,4,7], we give here only a short account. The measurements were carried out at the Jülich Cooler Synchrotron COSY using the time-of-flight spectrometer TOF located at one of its external beam lines. The TOF spectrometer is a modular detector setup, which can be adapted to the specific requirements of an experiment. Here it was used in its standard version for hyperon production, see *e.g.* Figs. 1 and 2 of Ref. [4]. At the entrance to the detector system the beam – focused to a diameter smaller than 2 mm – hits the thin-walled LH_2 target, which has a length of 4 mm, a diameter of 6 mm and 0.9 μm thick hostaphan foils as entrance and exit windows. At a distance of 22 mm downstream of the target the two layers of the start detector (each consisting of 1 mm thick scintillators cut into 12 wedge-shaped sectors) were placed. A silicon microstrip detector as well as two fiber hodoscopes were installed at distances 30, 100 and 200 mm from the target. These three tracking detectors provide the position information of the traversing charged particles, whereas the start detector supplies the start time signals for the time-of-flight (TOF) measurements. After a flight path of about 3 m through the evacuated vessel the charged particles are detected in the highly segmented stop detector system consisting of the triple-layered quirl and ring detectors as well as a single-layered 96-fold segmented barrel detector.

2.2 Particle identification and event reconstruction

In the experiment the trigger suitable for the selection of hyperon production events required two hits in the start detector and four hits in the stop detectors. This multiplicity jump from two to four specifically selects the production of neutral hyperons, which decay into charged products like the Λ decay process $\Lambda \to p\pi^-$, which happens with a branching fraction of 64%. Tracks of charged particles are reconstructed from straight-line fits to the hit detector elements in start, fiber and stop detectors. They are accepted as good tracks of primary particles (p, K^+), if they originate in the target. The secondary particles resulting from hyperon decay (p, π^-) form a V-shaped track pair originating from a secondary vertex downstream of the microstrip detector. Primary vertices, which are located within the target volume, were reconstructed with an accuracy of $\sigma_{x,y} = 0.25$ mm and $\sigma_z = 0.7$ mm. The secondary vertex from the Λ decaying downstream the microstrip detector and upstream the first hodoscope was reconstructed with accuracy of $\sigma_{x,y} = 1.5$ mm and $\sigma_z = 4.5$ mm.

In addition to the tracking information we use the TOF information of all four ejectiles of an event to determine their four-momentum vectors. For the particle identification a kinematic fit is applied, where all permutations of particle assignments are considered and the one with the best χ^2 is selected as the correct one. Since the kinematics of the light(π, K) and heavy (p) emitted particles is quite different, finding of the correct particle assignments actually is rather clear-cut. According to detailed Monte Carlo (MC) simulations the misidentification rate was in the order of a few percent only – in agreement with previous TOF results [2,4].

Fig. 1 depicts the two-dimensional plot of the invariant mass $M_{p\pi^-}$ of the Λ decay particles versus the primary particle pK^+-missing mass spectrum for MC simulation (top) and data (bottom). As can be seen the resolution in invariant and missing mass are comparable, and the MC simulation reproduces very well the experimental situation. The dashed circles in Fig. 1 indicate the region of events accepted for the subsequent analysis steps.

The kinematic fit was fivefold overconstrained, where the fifth overconstraint originates from the condition that the invariant mass of the four-momenta of the decay particles has to be identical to the Λ mass. A total of 30,000 events passed the criterion of $prob(\chi^2) > 10\%$ in the kinematic fit for being accepted as a proper event [23].

The primary particle pK^+ missing mass spectrum of the events finally selected by the χ^2 criterion is shown in Fig. 2 *before* the kinematic fit. The Λ peak appears with essentially no background and is in very good agreement with the Monte Carlo (MC) simulations of the detector performance. The slight mass shift of the peak between data and MC is due to imperfections in the energy calibration.

The MC simulations also have been used for efficiency and acceptance corrections of the data. We used for these simulations as input a model-description for the reaction of interest, which provides a good description of the experimental differential distributions – see discussion in section 4. We note, however, that since the TOF detector covers nearly the full phase space of the reaction – see the Dalitz plots in Fig. 3 – the differences in the corrections between model-based and pure phase MC simulations are only minor.

By use of the kinematic fit the mass resolution in the spectra of the invariant masses $M_{K\Lambda}$, M_{pK} and $M_{p\Lambda}$ (Fig. 4) improves from about 30 MeV/c^2 to 6 MeV/c^2 (FWHM).

The absolute cross section is obtained by relative normalization to literature data [25,26] for the elastic pp channel, which was measured in parallel during the experiment.

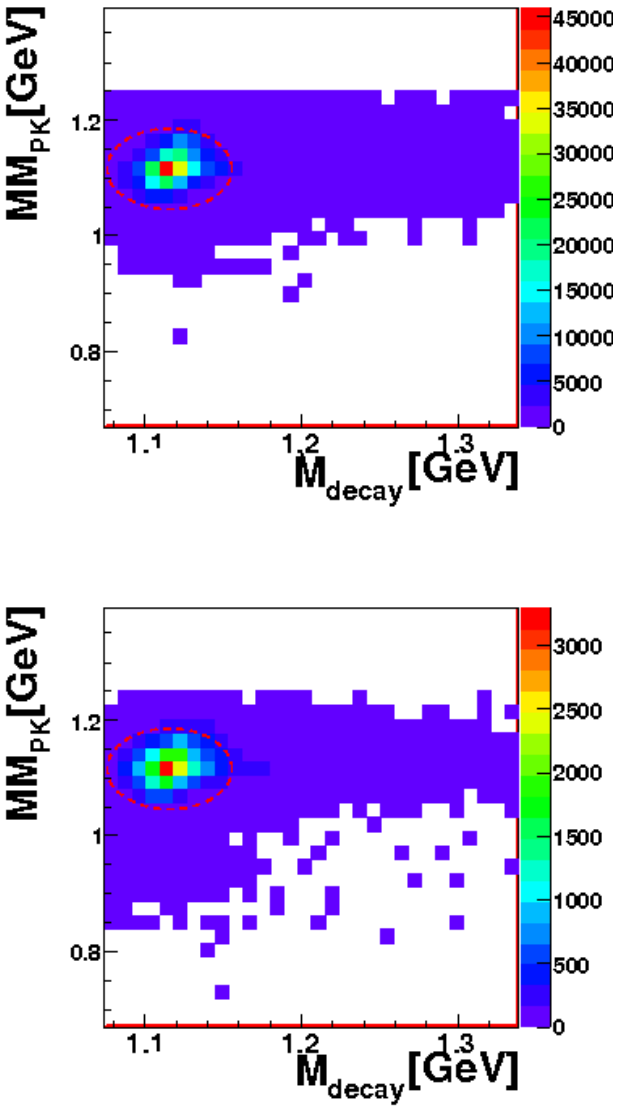

Fig. 1. Plot of the invariant mass $M_{p\pi^-} := M_{decay}$ of the Λ decay particles versus the primary particle pK^+-missing mass MM_{pK} for MC simulation (**top**) and data (**bottom**). The dashed circles indicate the range accepted for the subsequent kinematic fit. The scale of the z-axis is in arbitray units.

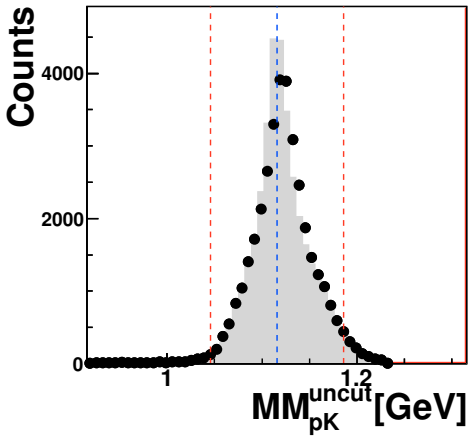

Fig. 2. pK^+-missing mass spectrum of events, which were finally selected as good candidates for the $pK^+\Lambda$ channel by the χ^2 criterion. The shaded area gives the MC simulation, the vertical middle line the position of the Λ mass and the two outer vertical lines the range accepted for the subsequent kinematic fit.

3 Results

For the total cross section of the $pp \to pK^+\Lambda$ reaction at 2.28 GeV we obtain $(21.2 \pm 0.2 \pm 2.0)$ μb, where the errors are statistical and systematic respectively. Within uncertainties this value agrees with that obtained in Ref. [2]. As in the previous TOF results [2,4,5,6] for the $pp \to pK^+\Lambda$ reaction the systematic uncertainty of about 10% is the by far dominant uncertainty. It originates from the uncertainties in the luminosity determination, reconstruction efficiency and acceptance correction.

Single differential cross sections are shown in Figs. 4 - 6. Fig. 3 exhibits the acceptance and efficiency corrected Dalitz plot of the three-body exit channel $pK^+\Lambda$. It is by no means homogeneous, *i.e.* phase space-like. The intensity in the Dalitz plot peaks at the left side of the short diagonal corresponding to high pK^+-invariant masses M_{pK^+}. In addition we see two vertical narrow structures corresponding to the $p\Lambda$-invariant masses $M_{p\Lambda}$ at threshold and at $M^2_{p\Lambda} \approx 4.54$ GeV$^2/c^4$ (see vertical arrows in Fig. 3), *i.e.* $M_{p\Lambda} \approx 2.13$ GeV$/c^2 \approx m_p + m_\Sigma$. The first structure may be related to the Λp FSI, whereas the latter one is in the region of the Σp production threshold.

In Fig. 4 we show the spectra of the three invariant mass systems $M_{K\Lambda}$, M_{pK} and $M_{p\Lambda}$ The data of all three strongly deviate from phase space, which is indicated by the shaded area in the plots. Among them the $M_{p\Lambda}$ spectrum appears particularly interesting, since it exhibits two narrow structures. They may be connected with FSI and ΣN cusp as mentioned above and will be discussed in the following.

4 Discussion

As shown in previous works [2,4,5,6], the gross features of the $pp \to pK^+\Lambda$ reaction may be well described by N^* resonance production with subsequent $N^* \to K^+\Lambda$ decay and by inclusion of the Λp FSI. The N^* resonances, which play a role here, are $N(1650)1/2^-$, $N(1710)1/2^+$ and $N(1720)3/2^+$. For the description of the data we assume excitation of these N^* resonances via t-channel meson exchange along the prescription given in Refs. [4,23]. The Σ cusp is treated in a simplified manner just as a nar-

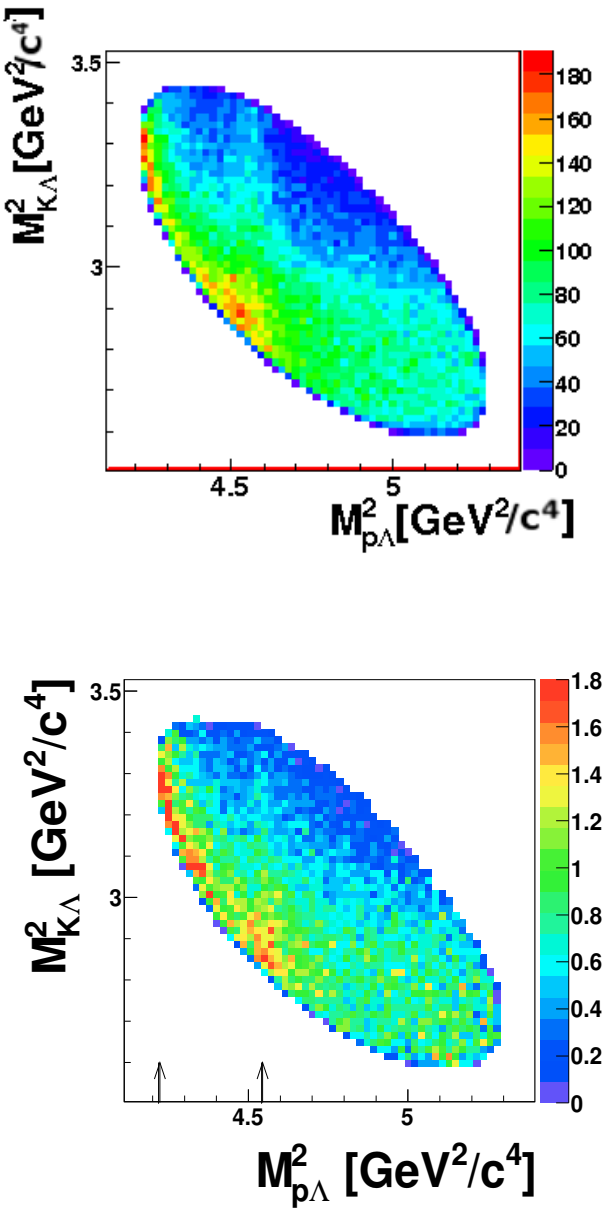

Fig. 3. Dalitz plot of $M^2_{K^+\Lambda}$ versus $M^2_{p\Lambda}$ for the $pp \to pK^+\Lambda$ reaction at $T_p = 2.28$ GeV, for MC simulation (**top**) and data (**bottom**). The two vertical narrow structures (see arrows) at the $p\Lambda$ threshold and at $M^2_{p\Lambda} = 4.54$ GeV$^2/c^4$ are due to the $p\Lambda$ FSI and the ΣN cusp, respectively. The scale of the z-axis is in arbitray units.

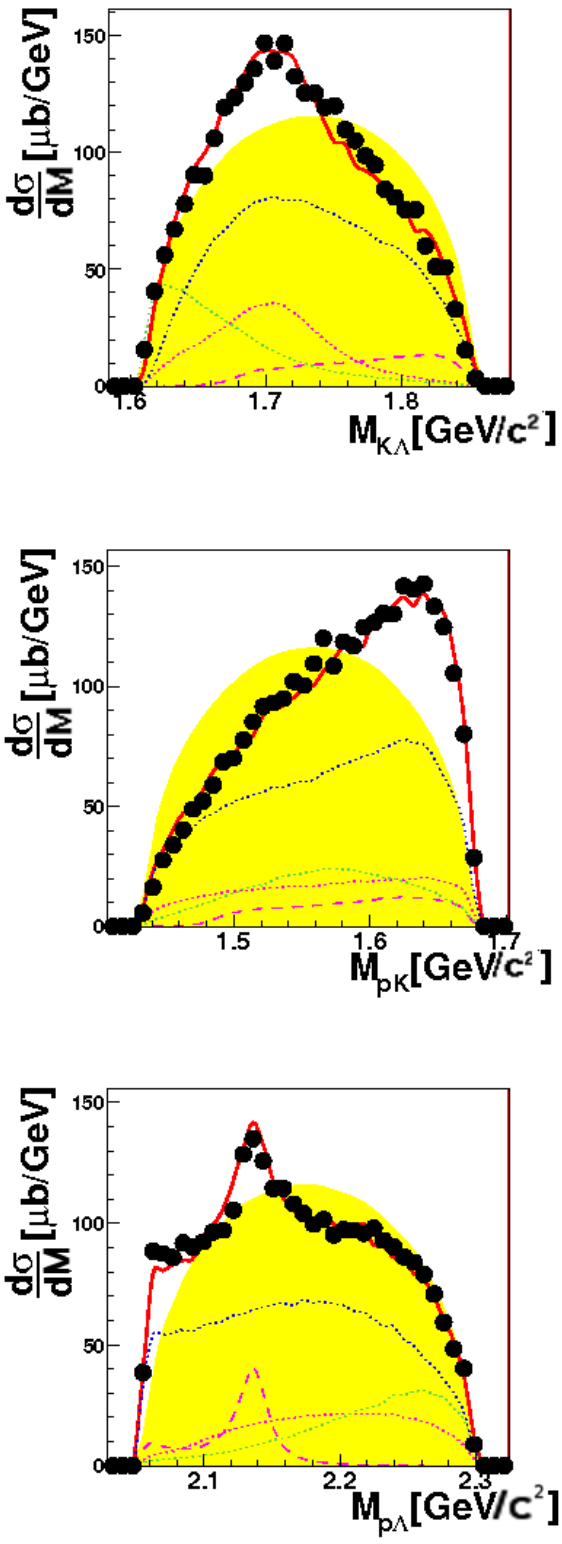

Fig. 4. Differential distributions of the invariant-mass systems $M_{K^+\Lambda}$ (**top**), M_{pK^+} (**middle**) and $M_{p\Lambda}$ (**bottom**). The shaded areas indicate phase-space distributions, the dotted lines the contributions of N^* resonances, the dashed line the Σ cusp effect and the solid line the full MC simulation.

row Λp resonance and the Λp FSI is taken into account in the factorization approximation of Ref. [1].

For the model fit to the data we allow mass and width of the N^* resonances to vary within the boundaries given in PDG [27]. In addition relative phase and strength parameter for each of the resonances have been fitted. For a quantitative description of the data in the FSI region we also need a readjustment of the FSI parameters resulting

Table 1. Results from the fit to the data for N^* resonances.

resonance	m_{N^*} (MeV)	Γ_{N^*} (MeV)	Φ_{N^*} (deg)	σ μb
$N(1650)1/2^-$	1653	168	29	3.5(4)
$N(1710)1/2^+$	1712	99	16	3.5(4)
$N(1720)3/2^+$	1731	383	0	12.8(13)

in $a_{\Lambda p}$ = -2.2 fm and $r_{\Lambda p}$ = 1.4 fm. These values are within 1σ and 2σ, respectively, of the HIRES result [1].

The result of a fit to the data is shown in Fig. 3, top, as Dalitz plot and in Fig. 4 by dotted (N^* resonances), dashed (Σ cusp) and solid (full calculation) lines. The resulting values for mass, widths and relative phase of the N^* resonances and Σ cusp are given in Table 1 in addition to their total cross section contributions. The data are reasonably well described by this fit. According to this analysis the enhancement (relative to phase space) in the $M_{p\Lambda}$ spectrum at the $p\Lambda$ threshold is predominantly due to the Λp FSI, whereas the enhancement at high $p\Lambda$ masses arises from N^* excitation, in particular from the excitation of $N(1650)1/2^-$ – see Fig. 4. A much more sophisticated Dalitz plot analysis in the framework of Ref. [28] taking into account all COSY-TOF data on this reaction is in progress. Hence we will not discuss the contribution of N^* resonances here further, but rather concentrate on the discussion of the cusp effect. The primary goal of the fit here is just to have a reasonable description of the data for the purpose of a reliable acceptance and efficiency correction by MC simulations – as discussed above in section 2 – and to also have some reliable estimate of the physical background (due to N^* resonances) underneath the Σ cusp. Also, as we see from the fit in Fig. 4, bottom, the assumption of a Breit-Wigner distribution for the Σ cusp is not a good description of this phenomenon.

In fact, since the cusp is a threshold phenomenon we do not expect a symmetric Breit-Wigner distribution, but an asymmetric energy dependence in form of a Flatté distribution [29]

$$d\sigma/dM_{\Lambda p} \;\sim\; \Gamma_{\Lambda p} \;/\; |m_R^2 - m_{\Lambda p}^2 - i m_R(\Gamma_{\Lambda p} + \Gamma_{\Sigma p})|^2$$

with

$$\Gamma_{\Lambda p} = g_{\Lambda p} q_{\Lambda p} \text{ and } \Gamma_{\Sigma p} = g_{\Sigma p} q_{\Sigma p},$$

where g_i and q_i are coupling constants and cm momenta, respectively, in the corresponding two-body subsystems. We have

$$q_{\Sigma p} = \frac{\sqrt{(m_{\Sigma p}^2 - (m_\Sigma + m_p)^2)(m_{\Sigma p}^2 - (m_p - m_\Sigma)^2)}}{2m_{\Sigma p}}$$

and

$$q_{\Sigma p} = i\frac{\sqrt{((m_\Sigma + m_p)^2 - m_{\Sigma p}^2)(m_{\Sigma p}^2 - (m_p - m_\Sigma)^2)}}{2m_{\Sigma p}}$$

above and below threshold, respectively.

If $g_{\Sigma N} \ll g_{\Lambda p}$ then the Flatté distribution approaches a symmetric distribution. If $g_{\Sigma N} \gg g_{\Lambda p}$ we have a very asymmetric distribution with a trailing slope at energies below the cusp and a rapid decline beyond the cusp. This situation is just opposite to what we observe in our data.

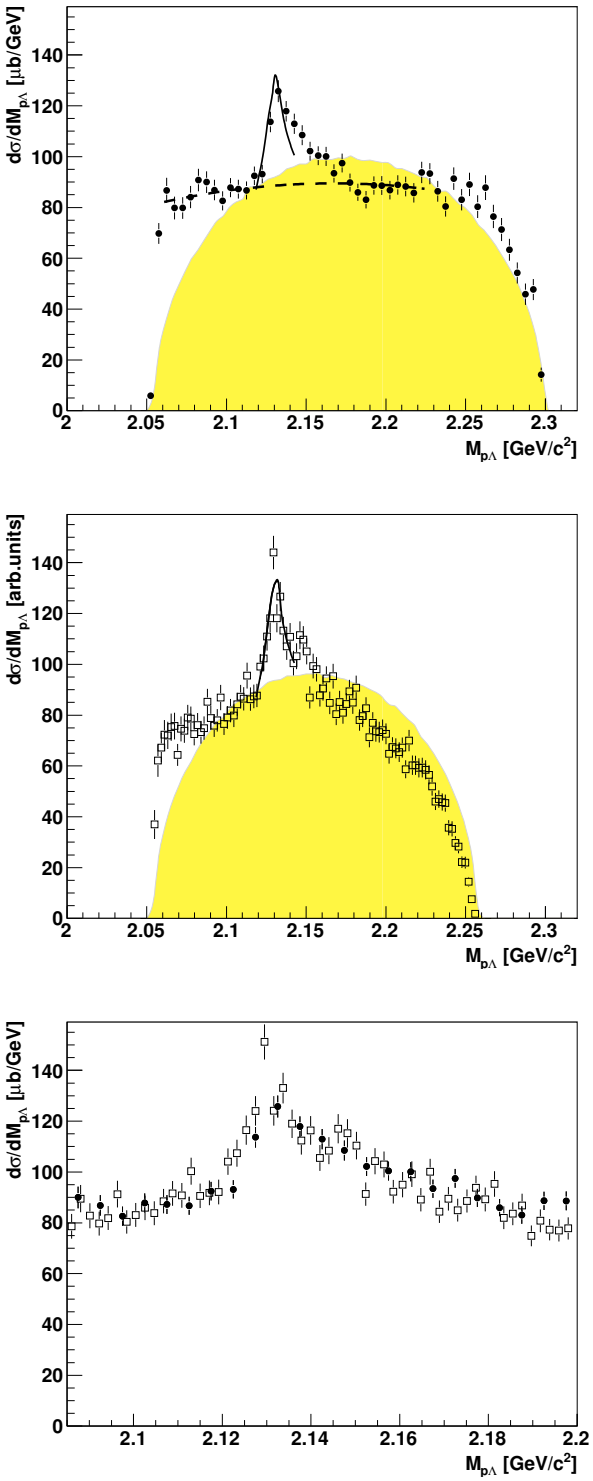

Fig. 5. Differential distribution of the invariant-mass system $M_{p\Lambda}$. The shaded area represents the phase-space distribution, the solid curve shows the shape of the cusp as obtained from a coupled-channel treatment [30], averaged over the experimental resolution and fitted in height to the data at the low-energy side of the cusp. The cusp is assumed to sit upon a smooth background represented by the dashed line. **Top**: data of this work taken at 3.081 GeV/c. **Middle**: data taken with the new straw tracker at 2.95 GeV/c, normalized arbitrarily [24]. **Bottom**: comparison of both data sets in the cusp region.

Also, a large $g_{\Sigma N}$ means a strong ΣN FSI, which in turn causes a strong low-mass enhancement in the ΣN invariant-mass spectrum as well as a steep increase of the total cross section near threshold of the $pp \to \Sigma NK$ reactions. Explicit measurements of these Σ production channels [2,3] provide no evidence for that. Since we have a sizeable Λp FSI, we hence expect $g_{\Sigma N} \ll g_{\Lambda p}$, *i.e.* a more or less symmetric distribution around the cusp. This is borne out also in a recent theoretical treatment of Λ and Σ production in NN collisions in the framework of the coupled channel effective range method [30]. The resulting cusp distribution folded with the appropriate experimental resolution is shown in Fig. 5 as solid curve. Similar to the prediction of Laget [15] we have the situation that the low-energy side agrees very well with the data, whereas the data on the high-energy side fall off much less steep than predicted.

In order to check whether the observed larger width is due to our experimental resolution, we compare in Fig. 5 our $M_{p\Lambda}$ data from the high-statistics run with a more recent COSY-TOF high-resolution measurement at 2.95 GeV/c [24], see Fig. 5, middle. This measurement was performed utilizing the new straw-tracker at COSY-TOF providing an invariant mass resolution of 2.6 MeV/c^2 FWHM, *i.e.* more than twice better than in this work. Both data sets are compared in Fig. 5, bottom, depicting the cusp region in enlargement. Aside from a possible slight shift of about 1 - 2 MeV/c^2, which is within the uncertainty of mass calibrations, both data sets coincide – in particular, if the different resolutions are taken into account. We see that both data sets exhibit the cusp in compatible shape and also size (relative to the background).

Admittedly, there appears to be possibly a slight difference. Whereas the high-statistics data exhibit a gentle decline at the high-energy side, the high-resolution data show the indication of a roughly 5 MeV broad bump upon the declining slope near 2.146 GeV/c^2. Since this bump effect may be less than 3σ – depending on the assumption of background – and hence not statistically significant, we do not want to speculate about its nature at this point. However, we would like to mention that already kaonic deuterium data suggested a two-bump scenario. In particular the bubble-chamber data with the highest statistics and a quoted mass resolution of σ = 1.0 - 2.6 MeV/c^2 [17] have been fitted by two symmetric Breit-Wigner functions with $m_1 = 2128.7 \pm 0.2$ MeV/c^2, $\Gamma_1 = 7.0 \pm 0.6$ MeV/c^2 and $m_2 = 2138.8 \pm 0.2$ MeV/c^2, $\Gamma_2 = 9.1 \pm 2.4$ MeV/c^2 suggesting two nearby resonance states separated by 10 MeV/c^2. The position of this second bump (shoulder) is, however, not compatible with the position of the unincisive bump at 2.146 GeV/c^2 in Fig. 5, middle and bottom. From this we conclude that at present there is no statistically solid evidence for a second bump beyond the ΣN cusp, however, there is a solid evidence for a surplus of cross section right beyond the cusp position, which so far is not understood theoretically.

The situation might change and the physical relevance of the second bump structure seen in Fig. 5, middle, might have to be re-discussed, if it should turn out that the cusp effect has indeed an energy dependence at the high-energy side as given by Refs. [15,30]. Having a width of only a few MeV, such a bump appears to be smeared out in our measurement with the coarser energy resolution shown in Fig. 5, top, producing there just a shoulder. Also, the differences between the two-resonance scenario of Tan *et al.* [17] and our results for cusp and second bump could be reconciled, if we allow to shift their resonance masses by 3 MeV/c^2, so that their first resonance coincides with the value for the ΣN threshold – as we find it for the position of the cusp in our data. That way the value for the second resonance mass in Ref. [17] would move to 2.142 GeV/c^2 and be no longer in serious disagreement with the position of the second bump in our high-resolution spectrum. For a new reinvestigation of this two-resonance scenario including the data of this work we refer to Ref. [33].

The different behavior at the high-mass end of the two data sets displayed in Fig. 5 is just due to the different beam energies: For the 2.95 GeV/c data the kinematic phase-space limit is 2.258 GeV/c^2, for the 3.08 GeV/c data the corresponding value is 2.299 GeV/c^2. In addition the influence of the broad N^* resonances, which determine the continuum below the cusp, depends on the beam energy – as demonstrated in Ref. [4].

As expected the cusp is located at $m_p + m_{\Sigma^0} = 2131$ MeV/c^2. This is consistent with the assumption that the observed structure corresponds to the production of Σ right at its threshold. In principle there should be two ΣN cusps, since $m_p + m_{\Sigma^0} = m_n + m_{\Sigma^+} + 2$ MeV/c^2. However, due to the finite invariant-mass resolution of the data we are unable to separate these. Since the excitation of N^* resonances gives a flat energy dependence in the $M_{p\Lambda}$ distribution, see Fig. 4, we assume the physical background not belonging to the cusp scenario to be represented by the dashed curve drawn in Fig. 5. Associating that way the surplus of cross section above the dashed line with the cusp scenario, *i.e.* neglecting possible interference effects, we obtain a cusp cross section, which corresponds to roughly 5% of the total $pp \to pK^+\Lambda$ cross section.

The cusp scenario has a variety of consequences, which can be tested experimentally by the cusp angular distributions. Such angular distributions are shown in Fig. 6. They have been obtained by subtraction of the background as shown in Fig. 5, however, now for each angular bin individually. *I.e.*, we split the double-differential cross section $d^2\sigma/dM_{p\Lambda}dcos\Theta$ into eight equidistant angular bins of $dcos\Theta$, fit then in each of these eight spectra a second-order polynomial to the data in the regions outside the cusp and integrate the strength in the cusp region above this polynomial line. This procedure of subtracting the background for each angular bin individually has been applied successfully already in previous TOF work, see *e.g.* Refs. [2,3], for a detailed presentation of this method see Ref. [31]. We note that a sideband background subtraction [23] leads so similar results, however, it is in general not as reliable.

Since the cusp effect is small compared to the background originating from N^* production, the cusp angular distributions have now substantial uncertainties, both sta-

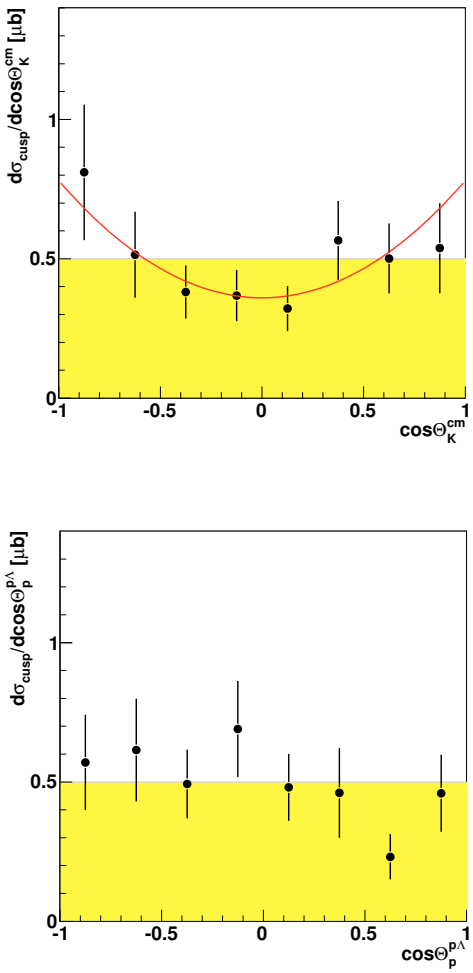

Fig. 6. Distribution of the ΣN cusp over the K^+ angle in the center-of-mass system $\Theta^{cm}_{K^+} = 180^\circ - \Theta^{cm}_{p\Lambda}$ (**top**) and over the proton angle in the $p\Lambda$ subsystem (Jackson frame) $\Theta^{p\Lambda}_p$ (**bottom**). The plotted error bars include both statistical and systematic uncertainties.The shaded areas denote phase-space distributions. The solid curve in the top figure represents a Legendre fit.

tistical and in particular systematic. The systematic errors have been studied by varying the background description with the second-order polynomial. As a result we find that the systematic uncertainty is up to four times as big as the statistical uncertainty. The latter is readily estimated from the fact that the cusp is just 1/20 of the total cross section. With a total of 30000 events and eight angular bins we have on average only somewhat more than 100 events left in the cusp of an angular bin spectrum, *i.e.* the statistical uncertainty is already in the 10% region.

The condition of the Σ being produced right at threshold means that the Σ and N are in relative s wave with the consequence that the spin-parity of the ΣN system right at threshold must be $J^P = 0^+$ or 1^+. Hence, the $p\Lambda$ system resulting from the ΣN system can only be in relative s- or d-waves. The observed proton angular distribution in the $p\Lambda$ subsystem (Jackson frame) within the ΣN cusp is compatible with $s-$wave phase-space, see Fig. 6, bottom. A dominant d-wave contribution would lead to a strongly anisotropic distribution. We note that the observed distribution is very different from the situation in the residual $pK^+\Lambda$ channel, where the corresponding Jackson frame distribution exhibits strong p-wave contributions – see Fig. 7 in Ref. [2].

The angular distribution of the K^+, shown in Fig. 6, top, is compatible with dominantly s-waves relative to the ΣN system, which is observed in our case as $p\Lambda$ system in the ΣN cusp. The p-wave component could be obtained from the Legendre fit to the data according to the ansatz

$$d\sigma/dcos\Theta^{cm}_K \;\sim\; a_0 + a_2(3\;\cos^2\Theta^{cm}_K - 1)/2,$$

where the parameters $a_0 = (0.50 \pm 0.10)$ μb and $a_2 = (0.28 \pm 0.09)$ μb. This result is different from the situation in the residual $pK^+\Lambda$ channel, however, very similar to that observed in the $pK^+\Sigma^0$ channel at the same incident energy, see Fig. 10 and Table 5 in Ref. [2], and it is qualitatively similar to the K^0 cm angular distribution measured in $pK^0\Sigma^+$ channel at 2.95 GeV/c [32].

As mentioned in the introduction the only other data on the ΣN cusp in pp induced K production originate from inclusive single-arm magnetic spectrometer measurements at Saclay [12] and COSY (HIRES collaboration [10]). In both cases essentially only a sharp increase in the cross section with a slight indication of a bump is seen in the K^+ missing mass spectrum at the Σp threshold. Since in these inclusive measurements Σ production cannot be separated from Λ production, the trailing slope of the ΣN cusp is not observed. If we compare these missing mass spectra to the $M_{p\Lambda}$ spectrum in Fig. 5 – though the latter contains the integration over all K^+ angles – we see that at least qualitatively the shape of the single-arm spectra is very close to that of the $M_{p\Lambda}$ spectrum up to the maximum of the ΣN cusp. This is true also for the height of the cusp relative to the $pK^+\Lambda$ continuum left from the cusp.

In Ref. [12] the cusp has been extracted from data at $T_p = 2.3$ GeV - which is close to our energy - by subtracting phase space distributions for Λ and Σ production – see Fig. 5 in Ref. [12]. As a result of this very crude treatment they obtain a bump at the cusp position, which indicates a width of roughly 10 MeV/c^2 – at variance with our findings of a much broader structure.

Also, the width of 20 MeV/c^2 observed now in exclusive measurements is much larger than the value of 3 MeV/c^2 assumed in Ref. [10] for the width of the ΣN cusp. Since the width of the ΣN cusp affects sensitively the value for the total cross section of the $pp \to nK^+\Sigma^+$ cross section extracted in Ref. [10] from the inclusive K^+ missing mass spectrum, the value of that cross section reduces substantially when accounting for the much larger width of the cusp extreacted here.

The calculations of Laget, which account for both Λ and Σ production as well as the ΣN cusp effect, are published only for specific K^+ scattering angles. This leaves

us merely with the possibility of a very qualitative comparison. In Refs. [12,15] the calculations are shown for a K^+ scattering angle of 10° at $T_p = 2.3$ GeV. Since the latter is close to the incident energy of this work, we may compare that calculation directly to the $M_{p\Lambda}$ spectrum in Fig. 5. From visual inspection we see that Laget's calculation qualitatively gives the right order of magnitude for this effect, however, the calculated cusp effect appears to be substantially narrower than observed in our data — as already mentioned above.

The cusp possibly may shed also new light onto the question about the ΣN-FSI. From differential and total cross section measurements of the $pp \to pK^+\Sigma^0$ reaction it has been concluded that there is no sizeable $\Sigma^0 p$-FSI [2]. The presence of the pronounced cusp observed in $pp \to pK\Lambda$ needs a different interpretation, since such a structure points to a very strong $\Sigma N \to \Lambda N$ transition. Therefore even at the threshold the ΣN interaction is strongly inelastic, which might well be the reason of diminishing any strong final state distortion in the excitation function for $pp \to NK\Sigma$. It is therefore particularly interesting to look into data on the $pp \to pK^0\Sigma^+$ reaction, where the ΣN final state is purely isospin 3/2 and therefore does not couple to the ΛN channel. In fact, differential and total cross section data for this channel have been taken recently at TOF [3]. They show no sign of any significant FSI effects. Following the argumentation above this means that there is no sizeable FSI in the I=3/2 channel – different to the situation in the I=1/2 channel. A thorough theoretical explanation of these findings is highly desirable. For recent data on that channel see Ref. [3] and references therein.

5 Summary

This work presents the first exclusive and kinematically complete measurements of the ΣN cusp effect in the $pp \to pK^+\Lambda$ reaction and establishes this phenomenon in proton induced Λ production for the first time. The data exhibit a pronounced asymmetric shape of the cusp, which is gently declining at its high-energy side. This is opposite to what is expected from a Flatté distribution. Due to the gentle fall-off at its high-energy side the cusp appears to be significantly broader than anticipated from theoretical predictions. Whether this is indicative of a narrow resonance above the cusp energy – as speculated in earlier measurements of kaonic deuterium and as also possibly suggested by the high-resolution data presented here, can not be decided at the present stage.

The measured angular distributions of the cusp point to s-waves between the kaon and the $p\Sigma$ system, as well as dominantly s-waves between the subsequently emerging Λ and proton. Detailed theoretical calculations for this cusp effect would be highly welcome in view of these new higher statistics measurements.

6 Acknowledgments

This work has been supported by BMBF, DFG (Europ. Graduiertenkolleg 683) and COSY-FFE (Forschungszentrum Jülich). We acknowledge valuable discussions with F. Hinterberger, H. Machner, A. Sibirtsev, H. Ströher and C. Wilkin.

References

1. A. Budzanowski *et al.*, Phys. Lett.**B 687**, 31 (2010).
2. M. Abdel-Bary *et al.*, Eur. Phys. J. **A 46**, 27 (2010), Erratum-ibid. A46, 435 (2010).
3. M. Abdel-Bary *et al.*, Eur. Phys. J. **A 48**, 23 (2012).
4. S. Abd El-Samad *et al.*, Phys. Lett.**B 688**, 142 (2010).
5. S. Abd El-Samad *et al.*, Phys. Lett.**B 632**, 27 (2006).
6. R. Bilger *et al.*, Phys. Lett.**B 420**, 217 (1998).
7. M. Abdel-Bary *et al.*, Phys. Lett.**B 649**, 252 (2007).
8. M. Abdel-Bary *et al.*, Phys. Lett.**B 595**, 127 (2004).
9. M. Nekipelov *et al.*, J. Phys. **G 34**, 627 (2007)
10. A. Budzanowski *et al.*, Phys. Rev.**D 84**, 032002 (2011); arXiv:1105.2281 [hep-ex].
11. T. Yamazaki *et al.*, Phys. Rev. Lett. **104**, 132502 (2010).
12. R. Siebert *et al.*, Nucl. Phys. **A 567**, 819 (1994).
13. J. Gasser, B. Kubis and A. Rusetsky, Nucl. Phys. **B 850**, 96 (2011); arXiv:1103.4273 [hep-ph].
14. A. Budzanowski *et al.*, Phys. Lett. **B 692**, 10 (2010).
15. J. M. Laget, Phys. Lett. **B 259**, 24 (1991).
16. O. I. Dahl *et al.*, Phys. Rev. Lett. **6**, 142 (1961).
17. T. H. Tan, Phys. Rev. Lett. **23**, 395 (1969).
18. O. Braun *et al.*, Nucl. Phys. **B 124**, 45 (1977).
19. R. H. Dalitz, Nucl. Phys. **A 354**, 101c (1981).
20. A. M. Badalyan, L. P. Kok, M. I. Polikarpov, Yu. A. Simonov, Phys. Rep. **82**, 31 (1982).
21. G. Toker, A. Gal and J. M. Eisenberg, Nucl. Phys. **A 362**, 405 (1981).
22. M. Torres, R. H. Dalitz and A. Deloff, Phys. Lett. **B 174**, 213 (1986).
23. K. Ehrhardt, PhD Thesis, Universität Tübingen, 2011;http://tobias-lib.uni-tuebingen.de/volltexte/2012/6021/pdf/final_
24. M. Röder, PhD Thesis, Ruhr-Universität Bochum , 2012; E. Borodina et al. (COSY-TOF Collaboration) to be published.
25. D. Albers *et al.*, Phys. Rev. Lett. **78**, 1652 (1997).
26. SAID data base http://gwdac.phys.gwu.edu/; R. A. Arndt *et al.*, Phys. Rev. **C 76**,025209 (2007).
27. Particle Data Group, Phys. Rev. **D 86**, (2012) 010001
28. A. Sibirtsev, J. Haidenbauer, H.-W. Hammer, S. Krewald, Eur. Phys. J. **A 27**, 269 (2006).
29. S. M. Flatteé, Phys. Lett. **B 63**, 224 (1976).
30. A. Sibirtsev *et al.*, to be published.
31. M. Abdel-Bary *et al.*, Eur. Phys. J. **A 16**, 127 (2003).
32. R. Dzhygadlo, PhD Thesis, Universität Bonn, 2012.
33. H. Machner et al., Nucl. Phys. **A**, in press; arXiv: 1301.6089 [nucl-ex].